ELSEVIER

Polymer 43 (2002) 3951–3957

polymer

www.elsevier.com/locate/polymer

Characterization of poly(vinylidenefluoride-*co*-hexafluoropropylene)-based polymer electrolyte filled with TiO_2 nanoparticles

Kwang Man Kim*, Nam-Gyu Park, Kwang Sun Ryu, Soon Ho Chang

Battery Technology Team, Electronics and Telecommunications Research Institute (ETRI), 161 Gajong, Yusong, Daejon 305-350, South Korea

Received 7 January 2002; received in revised form 7 March 2002; accepted 18 March 2002

Abstract

Nanoscale TiO_2 particle filled poly(vinylidenefluoride-*co*-hexafluoropropylene) film is characterized by investigating some properties such as surface morphology, thermal and crystalline properties, swelling behavior after absorbing electrolyte solution, chemical and electrochemical stabilities, ionic conductivity, and compatibility with lithium electrode. Decent self-supporting polymer electrolyte film can be obtained at the range of <50 wt% TiO_2. Different optimal TiO_2 contents showing maximum liquid uptake may exist by adopting other electrolyte solution. Room temperature ionic conductivity of the polymer electrolyte placed surely on the region of $>10^{-3}$ S/cm, and thus the film is very applicable to rechargeable lithium batteries. An emphasis is also be paid on that much lower interfacial resistance between the polymer electrolyte and lithium metal electrode can be obtained by the solid-solvent role of nanoscale TiO_2 filler.

Keywords: Polymer electrolyte; Poly(vinylidenefluoride); Titanium oxide nanoparticles

1. Introduction

Polymer electrolytes based on poly(vinylidenefluoride) (PVdF), in either immobilized liquid electrolyte (gel-type) or hybrid polymer membrane (porous-type), have been studied extensively and intensively to be capable of showing high ionic conductivity at room temperature and good mechanical property [1,2]. Of these, poly(vinylidene-fluoride-*co*-hexafluoropropylene) (P(VdF-HFP)) has been attracted as a highly promising material for the polymer electrolyte [3–14] of rechargeable lithium battery because of its high solubility and the lower crystallinity and glass transition temperature than PVdF. It was evenly confirmed that the P(VdF-HFP) used as a main substance of polymer electrolyte in the most commonly commercialized process of making plastic lithium-ion batteries (PLiON™) by Telcordia Technologies (formerly Bellcore) [15,16].

On the other hand, it has also been known that the addition of inorganic fillers such as alumina (Al_2O_3) and silica (SiO_2) to the polymer electrolyte led to the enhancement of physical strength as well as the increase in the absorption level of electrolyte solution. Recent studies of polymer electrolyte have a tendency toward the addition of nanoscale titania (TiO_2) particles to improve physical and electrochemical properties [17–20]; especially, to achieve an excellent compatibility with lithium electrode in poly(ethylene oxide)–lithium ionic salt systems. The nanoscale TiO_2 in the polymer electrolyte system was confirmed to play some useful roles in forming particle networks into polymer bulk (particle dispersion), inhibiting the crystallization and reorganization of polymer chains (solid plasticizer), and interacting with lithium ionic species (solid solvent). These features eventually resulted in the improvements of polymer electrolyte properties such as mechanical strength, ionic conductivity, electrochemical stability, cation transference number, lowering of interfacial resistance, and so on.

Combining both the concepts of polymer matrix and filler (i.e. P(VdF-HFP) and TiO_2) explained earlier, we prepare the porous P(VdF-HFP) films by varying the amount of TiO_2 nanoparticles and report the physical property changes of the films. We also show the changes in electrochemical properties of the polymer films before and after absorbing the lithium ionic salt-based electrolyte solution. Particularly explored through this paper is the evidence for the increase in ionic conductivity by TiO_2 addition and also discussed is an applicability to rechargeable lithium batteries.

2. Experimental

The P(VdF-HFP) used was a commercially available

* Corresponding author. Tel.: +82-42-860-6829; fax: +82-42-860-6836.
E-mail address: kwang@etri.re.kr (K.M. Kim).

0032-3861/02/$ - see front matter
PII: S0032-3861(02)00215-X

fluoro-copolymer, KynarFlex® 2801 (Elf Atochem N.A. Co.) which shares 12 mol% of hexafluoropropylene. The TiO_2 used was an anatase-type titanium oxide powder (PC-101, Titan Industry Co., Japan) which had high specific surface area of 340 m^2/g and average particle size of 20 nm. Supplier said the surfaces of PC-101 nanoparticles were passed through some hydrophilic treatment, and we worked on with the TiO_2 under ultralow-humidity condition (within a dry room). Prior to make the mixture, all the powder samples were dried in a vacuum oven at 150 °C for 12 h. The polymer films were prepared by dispersing the TiO_2 powder (0–2 g) by ultrasonication in 30 g of acetone solvent, adding slowly the P(VdF-HPF) powder (3–5 g), and milling the mixture. Here, the TiO_2 content was adjusted as 0, 5, 10, 20, 30, 40, and 50 wt% in the basis of the polymer film consisting of P(VdF-HFP) and TiO_2. The dispersion was carried out by a ultrasonicator (VibraCell™, Sonics and Materials Inc.) at the output amplitude of 35 W for 30 min, and the subsequent milling by a highly rotating ball-mill for 24 h at room temperature. The viscous slurry was cast on a clean glass plate using a doctor blade apparatus (with a gap of 400 μm) in a dry atmosphere (moisture content less than 0.1 ppm), and dried in a vacuum oven at 70 °C for 12 h. The self-supporting films were easily obtained with the thickness of 36–50 μm for all compositions of TiO_2 content. Here, we should say that the polymer films with >50 wt% TiO_2 exhibited a poor mechanical strength and a powder-like property (easily being crisp when dried), so that it failed to obtain a self-supporting film. The other films with lower content of TiO_2 than 50 wt% were easily obtained and processed to measure the properties.

Surface morphology of dried films was observed by a scanning electron microscope (Hitachi S800). For the films prepared, thermal properties were measured by a differential scanning calorimeter using a du Pont 2100 Thermal Analyst with a 910 Cell Base and crystalline properties by a Rigaku X-ray diffractometer using Cu $K\alpha_1$ radiation with the wavelength of $\lambda = 0.15406$ nm. Chemical instability and crystalline phase change of polymer component, which might occur by the TiO_2 addition, were also investigated by a Fourier-transform infrared spectrometer (Bomem MB-100) with the wavelength resolution of 4 cm^{-1}.

Pieces of film were then swollen for at least 24 h by absorbing the electrolyte solutions to give the polymer electrolyte films. Two electrolyte solutions were used in the present study: 1 M $LiClO_4$ dissolved in the 2:1 v/v mixture of ethylene carbonate (EC) and dimethyl carbonate (DMC) (1 M $LiClO_4$/EC–DMC) and 1 M $LiPF_6$ in the 1:1 v/v mixture of EC and diethyl carbonate (DEC) (1 M $LiPF_6$/EC–DEC). Prior to measure the liquid weight absorbed by the film, light-patting with a filter paper was done several times to remove the surface liquid. Thickness of swollen film after absorbing the liquid was within the range 42–60 μm.

Cyclic voltammetry test of the polymer electrolyte film was carried out on stainless steel electrode in a three-electrode cell (2 cm × 2 cm) in which lithium served as both the counter and the reference electrodes. A MacPile-II potentiostat/galvanostat system was used under the conditions of the scan rate of 10 mV/s and the potential range of 0–5 V vs. Li^+/Li. Ionic conductivity of the polymer electrolytes was determined from complex impedance spectra measured using a frequency response analyzer (Solartron HF 1225 Gain-Phase Analyzer) in the frequency range of 0.1 Hz to 100 kHz. A conductivity cell (2 cm × 2 cm) comprising two stainless steel electrodes on each side of the polymer electrolyte film was used. Temperature dependence data of ionic conductivity were also obtained over the range of 0–80 °C. The interfacial stability between lithium and polymer electrolyte was examined by monitoring the impedance of a 2 cm × 2 cm (Li/polymer electrolyte/Li) cell stored at room temperature as a function of time.

3. Results and discussion

3.1. Surface morphology

Fig. 1 shows the scanning electron microscope images of polymer film surfaces with different contents of TiO_2. As the TiO_2 content increases the film surface becomes rugged and the aggregates of fillers and polymer are partially observed. For the highly filled polymer films more than 30 wt% TiO_2, the nanoparticles are well dispersed and micro-pores distributed in part in the entire region of surface though some aggregates are still existed. This is from the imperfect dispersion of TiO_2 nanoparticles even severe condition such as ultrasonication and the subsequent ball-milling is

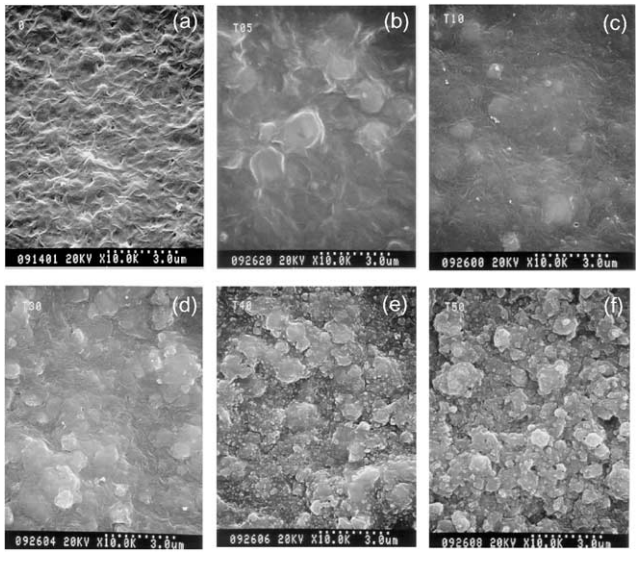

Fig. 1. Scanning electron microscope surface images (×10,000) of polymer films with different TiO_2 contents: (a) 0.0, (b) 5, (c) 10, (d) 30, (e) 40, and (f) 50 wt%. The 20 wt% sample is not shown because the trend of surface roughness is just on the middle between 10 and 30 wt% samples.

applied. That is to say, this is effectively from the affinity difference between the surface group of TiO_2 and the solvent molecule. Another emphasis should be put on the surface morphology affected by the interactions [21] between filler surface functionals and solvent/polymer molecules. Nevertheless, the present samples showing sufficiently rough surfaces with micro-sized aggregates and nanosized particles, which may be used as a porous-type polymer electrolyte [22] because of their own nature to absorb electrolyte solution (the liquid uptakes will be explained later when introducing Fig. 5).

3.2. Thermal and crystalline properties

Thermal behaviors of P(VdF-HFP) films filled with different content of TiO_2 are expected to exhibit the similar trend with those of the sole P(VdF-HFP) film, but only peak shifts at melting and/or crystallization temperature may be considered. As shown in Fig. 2, the melting temperatures on the heating run are almost same as 143–144 °C, irrespective of the TiO_2 content, but the heat of fusion decreases with the TiO_2 addition, which means the reduction of crystallinity of P(VdF-HFP). It is also noteworthy that heats of fusion for the samples having TiO_2 more than 30 wt% are almost same, which deviates greatly from that for P(VdF-HFP). This may be due to the fact that the crystal (α, β, γ, etc.) phases forming from polymer chain rearrangement are suppressed by the increased TiO_2 content when its content starts to exceed 30 wt%. Such changes in crystal state with increasing TiO_2 content have been re-examined from the result of Fourier-transform infrared spectroscopy (Fig. 4), which will be discussed later.

On the other hand, the effect of increasing TiO_2 content in the P(VdF-HFP)–TiO_2 films can be certainly confirmed by the cooling run results: as we previously investigated the thermal behaviors of the P(VdF-HFP)–SiO_2 systems [22], on cooling from the melt state the TiO_2 particles may play roles in nucleating agent and in accelerating the crystal growth. The crystallization point, however, shifts toward lower temperature with the increase in TiO_2 content: for instance, 126.6 °C for 5 wt% and 121.8 °C for 50 wt% TiO_2 sample. Difference in the crystallization temperatures is probably due to the inhibition of polymer crystal formation by the TiO_2 particle: that is, when the nanosized TiO_2 content becomes so large that the particles are densely distributed dominating the film, the TiO_2 no longer plays the role of accelerating the crystal growth by the narrowly neighboring particles. The more TiO_2 is included in the polymer film, the lower probability to crystallize at higher temperatures is given.

The transition of dominant crystal phases, with increasing TiO_2 content, from polymer chain arrangement into inorganic filler structure can be clearly observed by wide-angle X-ray diffraction patterns, as shown in Fig. 3. At low TiO_2 content, the films show some characteristic peaks (at $2\theta \approx 17$, 19, and 38°) of PVdF α-phase crystals [23,24] corresponding to big spherulites grown dominantly. Small spherulites such as γ-phase crystals may also be existed from the fact that the peak at $2\theta \approx 19°$ is corresponding to a mixture of (110) plane of α-phase and (021) of γ-phase [24]. Some data from infrared spectroscopy will be helpful in lighting up the existence of γ-phase crystals (Fig. 4). However, the peaks at $2\theta \approx 26$ and 36°, corresponding to (101) and (004) planes of anatase TiO_2 nanoparticles [25], respectively, are obviously pronounced with increasing TiO_2 content. Particularly, for the sample of 50 wt% TiO_2, all peaks given by the polymer chain crystals are almost

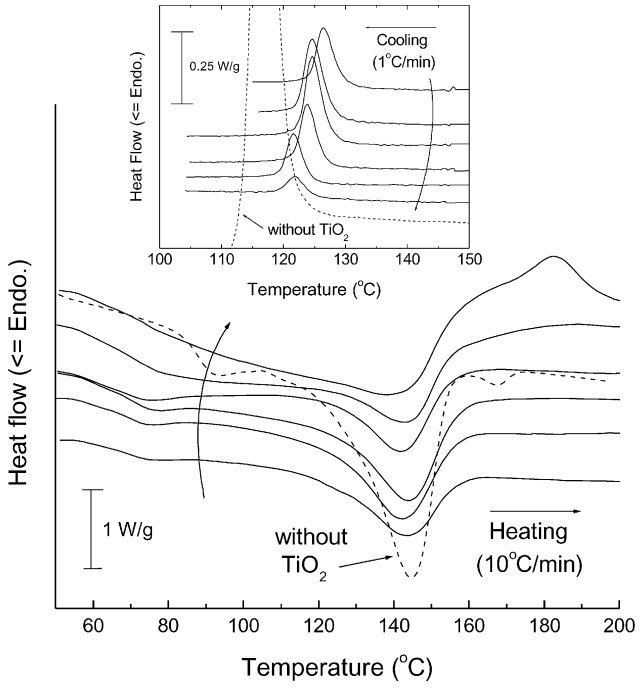

Fig. 2. Differential scanning calorimetric thermograms of the P(VdF-HFP)–TiO_2 films: results from heating run (rate 10 °C/min). The upper inset is from the cooling run (rate −1 °C/min). Arrows covering over the thermogram curves indicate 'increasing TiO_2 content' (5, 10, 20, 30, 40, 50 wt% in sequence).

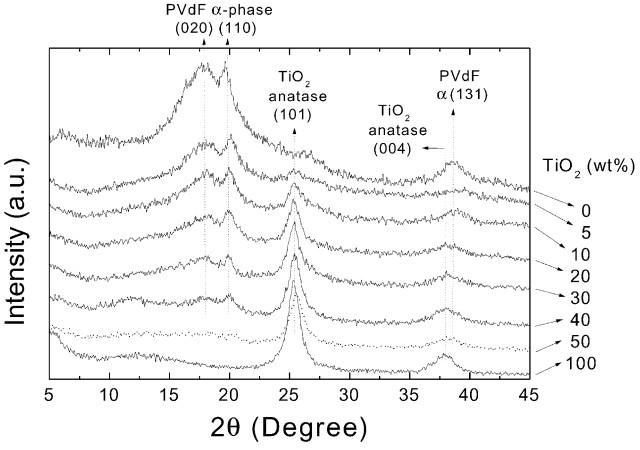

Fig. 3. Wide-angle X-ray diffraction spectra of the P(VdF-HFP)–TiO_2 films. As a reference, powder sample was only used for the TiO_2 100 wt%.

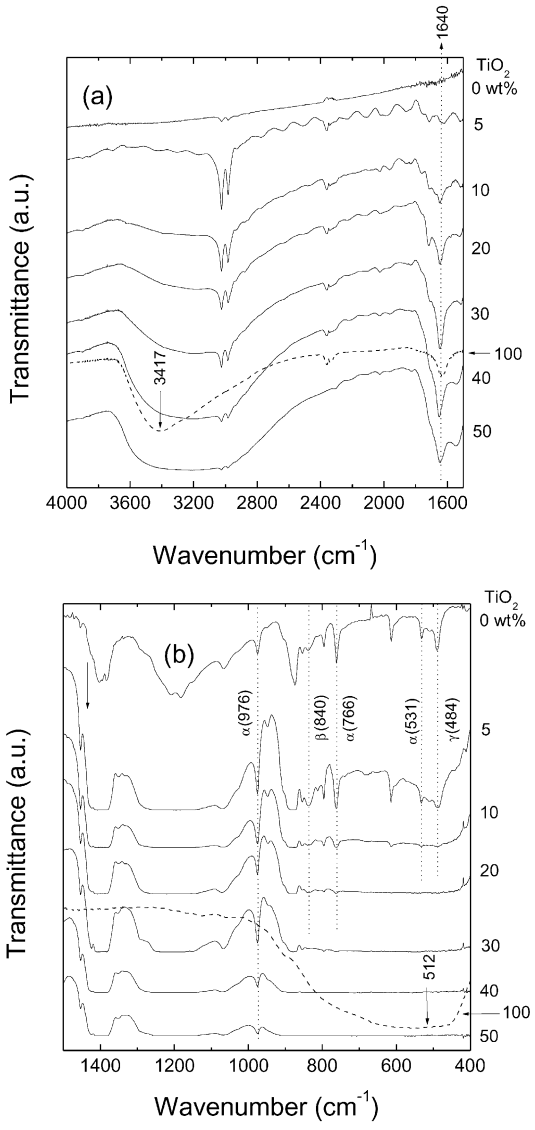

Fig. 4. Fourier-transform infrared spectra of the P(VdF-HFP)–TiO_2 films over the band ranges of (a) 4000–1500 and (b) 1500–400 cm^{-1}. As a reference, powder sample was only used for the TiO_2 100 wt%.

disappeared remaining a just small trace of (110) or (021) peak of PVdF α- or γ-phase. Thus, the crystallinity reflected by the polymer chain crystal only decreases greatly with the increase in the TiO_2 content.

These crystalline properties and the related identification of chemical species in P(VdF-HFP)–TiO_2 films can also be confirmed by Fourier-transform infrared spectra in Fig. 4. The strong vibrational bands at 531, 766, and 976 cm^{-1} are characteristic of the α-phase PVdF crystals, and the bands at 484 and 840 cm^{-1} correspond to γ- and β-phase PVdF crystals, respectively [23,26,27]. From Fig. 4(b), it is apparently seen that all these polymer crystal bands disappear with the increase in TiO_2 content. Only small portion of α-phase crystals, corresponding to the band at 976 cm^{-1}, remains. Comparing with the X-ray diffraction data, the remaining polymer crystals at high TiO_2 content can thus be identified as α-phase, not γ, and also its (110) plane is most distinguishable but other planes are somewhat broken or out of shape.

On the other hand, comparing with the infrared spectrum of anatase TiO_2 powder, all the P(VdF-HFP)–TiO_2 films do not show any Ti–O band, whereas the broad band of 800–450 cm^{-1} corresponds to the stretching mode vibration of Ti–O [28] and the band peak at 512 cm^{-1} the characteristic of Ti–O anatase crystalline phase [29]. However, the hydrous nature produced after the surface treatment of TiO_2 is reflected to the P(VdF-HFP)–TiO_2 films showing the bending mode of adsorbed water at 1640 cm^{-1} [30]. The water molecules originated from TiO_2 powder can be checked by the OH stretching vibration band for TiO_2 at 3417 cm^{-1} [29].

3.3. Liquid absorption and ionic conductivity

The liquid uptake (%) of polymer film has been determined by a weight increase rate as $(W_2 - W_1) \times 100/W_1$, where W_1 and W_2 are the weights of polymer films before and after absorbing the electrolyte solution, respectively. As expected, the P(VdF-HFP)–TiO_2 film absorbs different amounts of liquid with respect to the absorbing time, the kind and content of inorganic filler, and even the kind of electrolyte solution. For the case of absorbing the solution of 1 M $LiClO_4$/EC–DMC, the polymer films absorb rapidly more than half the saturated amounts within 10 min, and then mostly saturated after about 20 h (Fig. 5(a)). The sample having 20 wt% TiO_2 shows a maximum liquid uptake of ~77%, which is higher than the case of polymer films with fumed silica particles [22]. When using 1 M $LiPF_6$/EC–DEC as an electrolyte solution, the liquid uptake is faster than the former case and saturates within 6 h (Fig. 5(b)). Conditions of including 10 wt% TiO_2 and 6 h are sufficient to obtain the maximum liquid uptake, though its absolute value is similar to the former case.

Conductivities of the polymer electrolytes were calculated from the bulk resistances determined from complex impedance spectra. As shown in Fig. 6, the ionic conductivities of polymer electrolytes containing TiO_2 nanoparticles exhibit 1–2 order of magnitude higher than those of polymer electrolyte containing fumed silica particles [22]. Moreover, 1 M $LiPF_6$/EC–DEC in the polymer–TiO_2 matrix shows apparently higher ionic conductivity than 1 M $LiClO_4$/EC–DMC over all the specified temperature range and the TiO_2 content range tested. Highest conductivities are obtained for 20–30 wt% TiO_2 sample in case of 1 M $LiClO_4$/EC–DMC, and for 10–20 wt% TiO_2 sample in case of 1 M $LiPF_6$/EC–DEC. Here, it should be noted that these optimum TiO_2 contents showing highest conductivities are very consistent with those of exhibiting maximum liquid uptakes for each electrolyte solution. Nevertheless, it is very meaningful that room temperature ionic conductivities of the P(VdF-HFP)–TiO_2 are almost

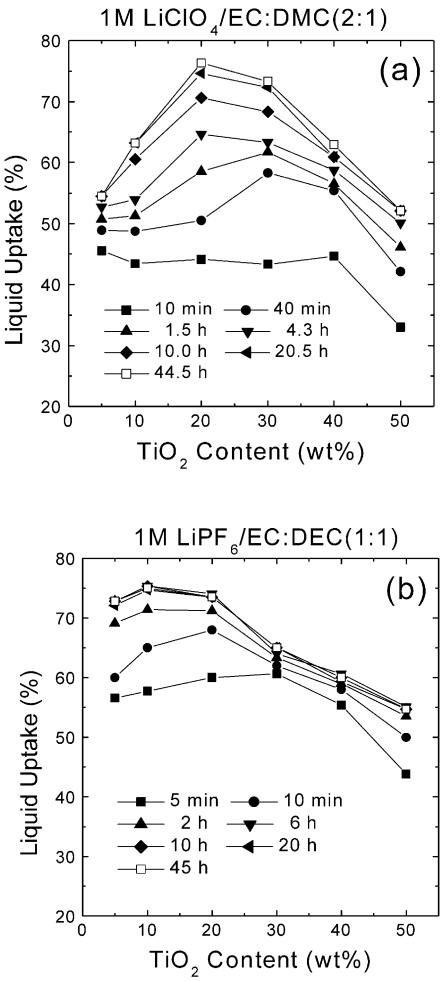

Fig. 5. Liquid uptakes of the P(VdF-HFP)–TiO_2 films, determined by the difference in weights of polymer films before and after absorbing the electrolyte solutions of (a) 1 M $LiClO_4$/EC–DMC (2:1 vol) and (b) 1 M $LiPF_6$/EC–DEC (1:1 vol).

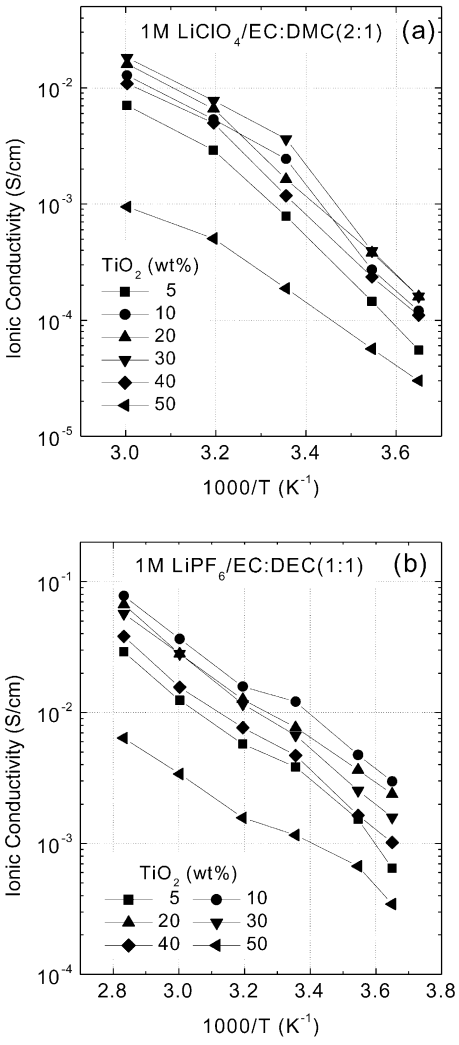

Fig. 6. Temperature dependences of ionic conductivity for the polymer electrolytes as functions of TiO_2 content when using the liquid solutions of (a) 1 M $LiClO_4$/EC–DMC (2:1 vol) and (b) 1 M $LiPF_6$/EC–DEC (1:1 vol).

higher than 10^{-3} S/cm which is adequate to apply to the polymer electrolyte for rechargeable lithium batteries.

Besides, the temperature dependence of ionic conductivity for the polymer electrolyte shows slightly different behaviors with respect to the electrolyte solution used. The polymer electrolyte using 1 M $LiClO_4$/EC–DMC obeys an empirical Vogel–Tammann–Fulcher (VTF) rule [31] rather than Arrhenius-type behavior whereas the system of using 1 M $LiPF_6$/EC–DEC does the opposite trend. In principle, the Arrhenius-type behavior means that the conductive environment of lithium cation in the polymer electrolyte is liquid-like and unchanged in the tested temperature region [32]. Whereas, the VTF rule mainly considers the deviation from the Arrhenius behavior, which may be explained by the partial crystallinity or the different relative fractions of crystalline and amorphous regions within the polymer electrolyte system [33].

From the earlier results, the basis for higher liquid absorption and enhanced ionic conductivity may explained as follows. The nanosized TiO_2 particles seem to facilitate localized influences, on associating polymer component, that retards the crystallization of the rigid vinylidenefluoride unit and that simultaneously preserves the amorphous structure of flexible hexafluoropropylene spacer unit. Thus micro- or nano-pores may be produced near the TiO_2 particles by the difference of interaction intensity with each units of polymer component. As a result, the TiO_2 particle shrinks the polymer matrix to produce heterogeneous pore distribution. In addition, the hydrophillicity of TiO_2 surface groups may be responsible for the higher liquid absorption and the resistivity to liquid leakage out of the polymer electrolyte.

3.4. Electrochemical stability and interfacial resistance

Fig. 7 compares cyclic voltammograms of the polymer electrolyte systems of using different electrolyte solutions. For the system of using 1 M $LiClO_4$/EC–DMC (Fig. 7(a)),

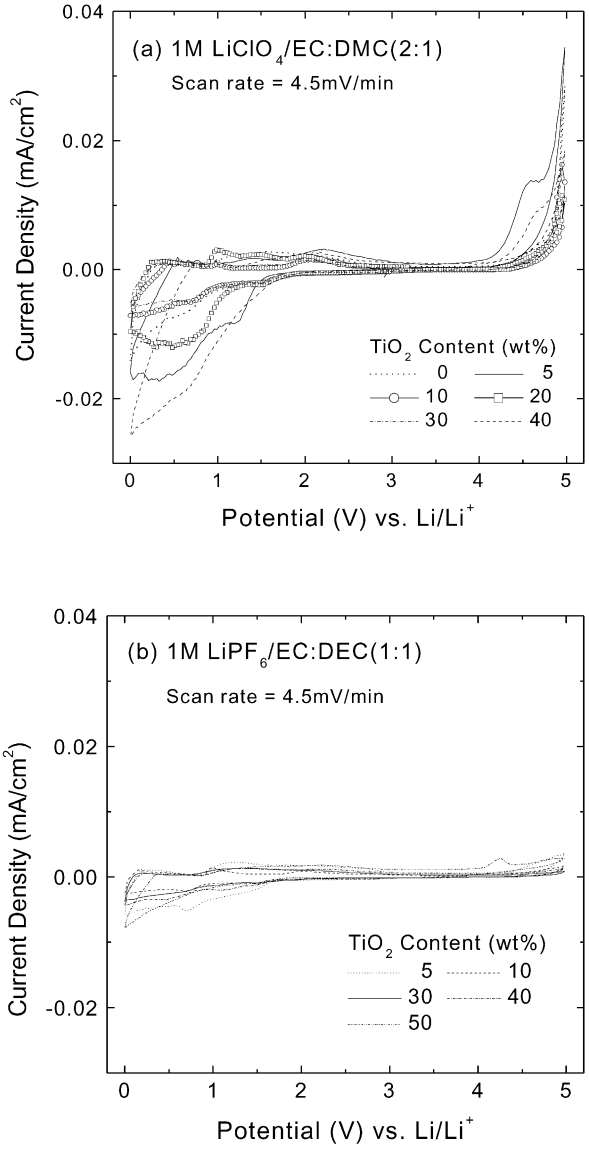

Fig. 7. Cyclic voltammograms of the polymer electrolytes on the working electrode of stainless steel: the electrolyte solutions used are (a) 1 M $LiClO_4$/EC–DMC (2:1 vol) and (b) 1 M $LiPF_6$/EC–DEC (1:1 vol).

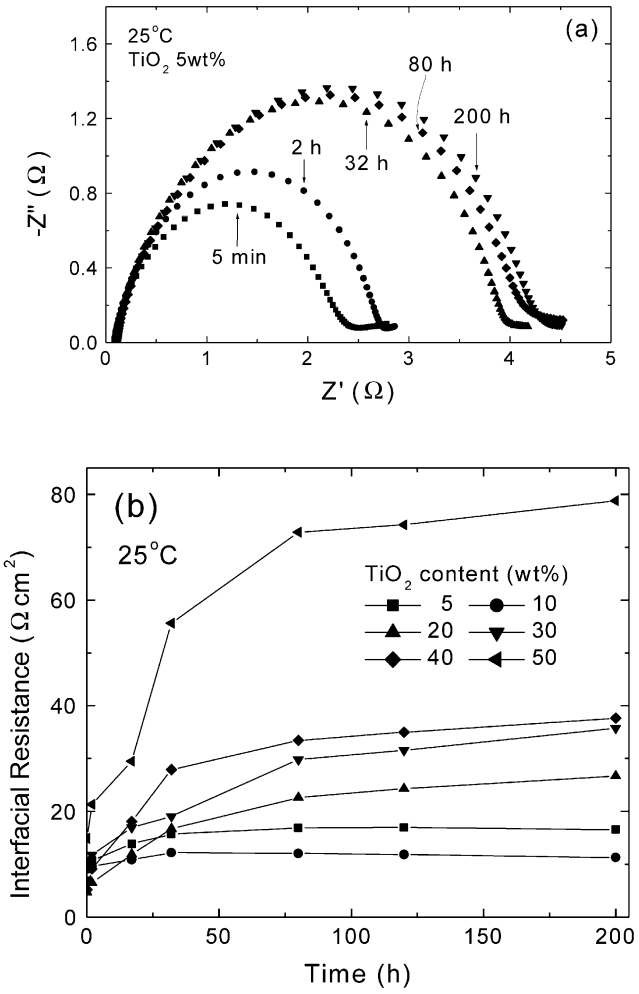

Fig. 8. (a) Impedance spectra of the polymer electrolyte, which is containing 5 wt% of TiO_2 and 1 M $LiPF_6$/EC–DEC (1:1 vol), on lithium electrodes as a function of time. (b) Time evolutions of interfacial resistances between the polymer electrolytes and lithium electrode.

the cathodic stability is moderately good without any electrochemical oxidation until the potential reaches 4.2 V. The polymer electrolyte with 5 wt% TiO_2 shows a higher pre-oxidation wave at 4.5 V, while others are slightly or hardly oxidized until 5.0 V. Compared to the gel-type P(VdF-HFP) electrolytes [34] without adding any filler, these oxidation potential windows are very narrow but they still have a possibility to be used for lithium rechargeable batteries whose operating voltage is in the range of 0–4.2 V. On the other hand, another effect of nanoscale TiO_2 addition can also be observed by the cyclic voltammograms in the low potential range, in which the interaction between the polymer electrolyte and lithium electrode must be considered as the plating (corresponding to anodic peak) and stripping (to cathodic peak) of lithium. As shown in Fig. 7(a), the stripping responses are decreased with increasing the TiO_2 content. The decrease in lithium stripping peak as current response may be thought as a result of interaction between nanoparticle surfaces and lithium cation, i.e. somewhat close association of Li^+ with TiO_2 surfaces [35], and then surely it leads to the stabilized interface occurring the weak current response between polymer electrolyte and lithium electrode. Also, it seems to be agreed well with the fact that TiO_2 nanoparticles in the polymer electrolyte matrix may play as well a role of enhancing the interfacial stability with lithium metal electrode or lithium cycling efficiency [17–19,35,36].

In contrast, the system of using 1 M $LiPF_6$/EC–DEC shows very small cathodic (<0.003) and anodic (<0.01 mA/cm^2) responses than the former case. The electrochemical stability in the potential range of 0–5 V can be much more reinforced by adopting the 1 M $LiPF_6$/EC–DEC as an electrolyte solution to the P(VdF-HFP)–TiO_2 polymer electrolyte system.

Fig. 8 presents the evolutions of impedance spectra and the resulted interfacial resistances of the polymer electrolyte when using 1 M $LiPF_6$/EC–DEC in a non-blocking cell with two lithium metal sheets. In the typical impedance spectra for the polymer electrolyte system as shown in Fig. 8(a), one semicircle grows with time and after certain period the growth becomes diminished, which means that a passivation layer is generated, developed by the interactions between polymer electrolyte components and lithium surface, and finally stabilized by the nanoscale TiO_2 particles. The interfacial resistance may be determined from diameter of the semicircle. As a result, the polymer electrolyte with 10 wt% TiO_2 is proved to be the best ($\sim$10 Ω cm^2 at 200 h) in the long-term stability with the lithium electrode. The estimated interfacial resistance is about 40 times lower than the case of using fumed silica particles [22].

4. Concluding remarks

The results reported here show that the P(VdF-HFP)-based polymer electrolyte can improve much more its physical and electrochemical properties by the addition of nanoscale TiO_2 particles. Particularly, some points may be taken as conclusions: (i) dispersion of nanoscale TiO_2 particles in the mixture is so difficult to require severe mixing conditions, (ii) free-standing polymer films are very hard to obtain if TiO_2 content exceeds $\sim$50 wt%, (iii) optimal TiO_2 contents for the maximum uptakes of electrolyte solution are found to be $\sim$20 wt% when using 1 M $LiClO_4$/EC–DMC (2:1 vol) and $\sim$30 wt% when using 1 M $LiPF_6$/EC–DEC (1:1 vol), (iv) the related electrochemical properties such as ionic conductivity, electrochemical stability, compatibility with lithium electrode, etc. show higher improvements in the range of the optimal TiO_2 content, and finally (v) the lowering of interfacial resistance is highly attributed to the solid-solvent role of nanoscale TiO_2 filler even though the present system is a porous-type polymer electrolyte.

References

[1] Voice AM, Southall JP, Rogers V, Matthews KH, Davies GR, McIntyre JE, Ward IM. Polymer 1994;35:3363.
[2] Voice AM, Davies GR, Ward IM. Polym Gels Networks 1997;5:123.
[3] Dai H, Zawodzinski TA. J Electroanal Chem 1998;459:111.
[4] Osaka T, Komada S, Uchida Y, Kitahara M, Momma T, Eda N. Electrochem Solid State Lett 1999;2:215.
[5] Osaka T, Kitahara M, Uchida Y, Momma T, Nishimura K. J Power Sour 1999;81–82:734.
[6] Stallworth PE, Fontanella JJ, Wintersgill MC, Scheidler CD, Immel JJ, Greenbaum SG, Gozdz AS. J Power Sour 1999;81–82:739.
[7] Arcella V, Sanguineti A, Quartarone E, Mustarelli P. J Power Sour 1999;81–82:790.
[8] Saito Y, Kataoka H, Capiglia C, Yamamoto H. J Phys Chem B 2000;104:2189.
[9] Saito Y, Capiglia C, Yamamoto H, Mustarelli P. J Electrochem Soc 2000;147:1645.
[10] Capiglia C, Saito Y, Kataoka H, Kodama T, Quartarone E, Mustarelli P. Solid State Ionics 2000;131:291.
[11] Michot T, Nishimoto A, Watanabe M. Electrochim Acta 2000;45:1347.
[12] Wang H, Huang H, Wunder SL. J Electrochem Soc 2000;147:2853.
[13] Song JY, Wang YY, Wan CC. J Electrochem Soc 2000;147:3219.
[14] Abbrent S, Plestil J, Hlavata D, Lindgren J, Tegenfeldt J, Wendsjö Å. Polymer 2001;42:1407.
[15] Tarascon J-M, Gozdz AS, Schmutz CN, Shokoohi F, Warren PC. Solid State Ionics 1996;86–88:49.
[16] Gozdz AS, Schmutz CN, Tarascon J-M, Warren PC. US Patent 5,418,091; 1995.
[17] Croce F, Appetecchi GB, Persi L, Scrosati B. Nature 1998;394:456.
[18] Croce F, Curini R, Martinelli A, Persi L, Ronci F, Scrosati B, Caminiti R. J Phys Chem B 1999;103:10632.
[19] Appetecchi GB, Croce F, Persi L, Ronci F, Scrosati B. Electrochim Acta 2000;45:1481.
[20] Scrosati B, Croce F, Persi L. J Electrochem Soc 2000;147:1718.
[21] Croce F, Persi L, Scrosati B, Serraino-Fiory F, Plichta E, Hendrickson MA. Electrochim Acta 2001;46:2457.
[22] Kim KM, Ryu KS, Kang S-G, Chang SH, Chung IJ. Macromol Chem Phys 2001;202:866.
[23] Prest Jr WM, Luca DJ. J Appl Phys 1978;49:5042.
[24] Marand HL, Stein RS, Stack GM. J Polym Sci, Part B: Polym Phys 1988;26:1361.
[25] Park N-G, Schlichthörl G, van der Lagemaat J, Cheong HM, Mascarenhas A, Frank AJ. J Phys Chem B 1999;103:3308.
[26] Kobayashi M, Tashiro K, Tadokoro H. Macromolecules 1975;8:158.
[27] Gregorio Jr R, Cestari M. J Polym Sci, Part B: Polym Phys 1994;32:859.
[28] Nyquist RA, Kagel RD. Infrared spectra of the inorganic compounds. New York: Academic Press, 1971. p. 214–5.
[29] Ivanova T, Harizanova A. Solid State Ionics 2001;138:227.
[30] Musić S, Gotić M, Ivanda M, Popović S, Turković A, Trojko R, Sekulić A, Furić K. Mater Sci Engng B 1997;47:33.
[31] MacCullum JR, Vincent CA, editors. Polymer electrolyte reviews. Amsterdam: Elsevier, 1989.
[32] Wen T-C, Chen W-C. J Power Sour 2001;92:139.
[33] Binesh N, Bhat SV. J Polym Sci, Part B: Polym Phys 1998;36:1201.
[34] Christie AM, Christie L, Vincent CA. J Power Sour 1998;74:77.
[35] Chung SH, Wang Y, Persi L, Croce F, Greenbaum SG, Scrosati B, Plichta E. J Power Sour 2001;97–98:644.
[36] Croce F, Persi L, Ronci F, Scrosati B. Solid State Ionics 2000;135:47.